STM JOURNALS

Journal of
Polymer & Composites

ISSN: 2321-2810 (Online)
ISSN: 2321-8525 (Print)
Volume 13, Special Issue 1, 2025
DOI (Journal): 10.37591/JoPC

https://journals.stmjournals.com/jopc

Research JoPC

Structural and Optical Properties of Nanocomposites of Polyethylene Oxide Embedded with Nano-ZnO

K. Sudhakar[1], R. Venugopal [2], N. Narsimlu [3], CH. Srinivas [4],*

Abstract

Polymer nanocomposites have attracted significant attention in recent years owing to their unique properties and potential applications in a variety of fields. In this study, PEO-ZnO nanocomposites were prepared with different wt.% (5, 10 and 15) nano-ZnO particles incorporated into PEO matrix by a solution casting method. Structural and Optical properties of PEO-ZnO nanocomposites were studied. X-ray diffraction (XRD) studies suggest the incorporation of ZnO NPs into PEO matrix. The XRD results confirm successful incorporation of ZnO NPs into PEO matrix without any additional impurity peaks. The 'XRD results' also revealed that the ZnO NPs were in the wurtzite phase. The presence of a peak at 2θ = 19.36° indicates semi-crystalline nature of PEO base matrix. The mean size of the ZnO NPs was determined to be approximately 52nm. The vibration bands observed in the prepared films were confirmed using Fourier transform infrared (FTIR) spectroscopy. The presence of NPs in the films was further investigated using FESEM. UV–visible optical absorption spectra were recorded to determine band gap values of prepared films. The band gap for pure PEO was 5.35eV, and this value decreased with increasing wt. % ZnO NPs due to change in band structure of pure PEO. The 'optical dielectric properties' were also evaluated, and optical dielectric constant increased with increasing wt.% ZnO NPs, which was attributed to the increase in density of states leading to the formation of polarization. The optical conductivity of prepared nanocomposites increases with increasing wt.% ZnO NPs due to formation of a charge-transfer complex. The obtained results indicate that the addition of ZnO NPs reduces optical band gap of PEO/ZnO nanocomposites.

Keywords: Nano ZnO, Solution casting, PEO-ZnO nanocomposites, XRD and FTIR studies, Optical properties.

INTRODUCTION

***Author for Correspondence**
CH. Srinivas

[1]Research Scholar, Department of Physics, University College of Science(A), Osmania University, Hyderabad, Telangana, India
[2]Research Scholar, Department of Physics, University College of Science(A), Osmania University, Hyderabad, Telangana, India
[3]Associate Professor, Department of Physics, University College of Engineering(A), Osmania University, Hyderabad, Telangana, India
[4]Professor, Department of Physics, University College of Engineering (A), Osmania University, Hyderabad, Telangana, India

Received Date: March 19, 2024
Accepted Date: August 20, 2024
Published Date: December 09,2024

Citation: K. Sudhakar, R. Venugopal, N. Narsimlu, CH. Srinivas. Structural and Optical Properties of Nanocomposites of Polyethylene Oxide Embedded with Nano-ZNO. Journal of Polymer & Composites. 2025; 13(Special Issue 1): S586–S600p.

In recent years, the field of nanotechnology has undergone remarkable advancements, revolutionizing various industries and opening up new possibilities for scientific exploration. One such area of interest is the development of polymer nanocomposites, which combine the unique properties of polymers with the enhanced characteristics of nanoparticles. Among these nanocomposites, polyethylene oxide (PEO) nanocomposites have garnered significant attention due to their exceptional properties and potential applications in diverse fields. The PEO polymer exhibits excellent solubility in water and other polar solvents. It has a high molecular weight, making it an ideal candidate for various applications. When PEO is combined with nanoparticles, such as clay, carbon nanotubes, or metal oxides, nanocomposites that exhibit enhanced mechanical, thermal, and electrical properties can form compared to those of pure PEO.

Owing to the unique properties of PEO nanocomposites, they are highly versatile and applicable in numerous fields. One of the most significant advantages of PEO nanocomposites is their improved mechanical strength and toughness. The presence of nanoparticles within the PEO matrix enhances its resistance to deformation and increases its load-bearing capacity. This property makes PEO nanocomposites suitable for structural material applications, such as aerospace components, automotive parts, and sports equipment. PEO nanocomposites exhibit excellent thermal stability and flame retardancy. The addition of nanoparticles acts as a barrier, preventing the propagation of heat and flame. This property makes PEO nanocomposites ideal for use in fire-resistant coatings, electrical insulation, and flame-retardant textiles. In addition to their mechanical and thermal properties, PEO nanocomposites also possess enhanced electrical conductivity. The incorporation of conductive nanoparticles, such as carbon nanotubes or metal oxides, into the PEO matrix facilitates the movement of charge carriers, resulting in improved electrical conductivity. This property makes PEO nanocomposites suitable for applications in electronic devices, energy storage systems, and sensors.

In recent years, the combination of polyethylene oxide (PEO) and zinc oxide (ZnO) nanoparticles has gained significant attention in the field of nanocomposite research. PEO, a polymer with excellent film-forming properties, and ZnO, a semiconductor with remarkable optical and electrical properties, form a synergistic combination that offers numerous advantages in various applications. ZnO nanoparticles exhibit unique optical properties, such as high transparency and ultraviolet (UV) absorption. When incorporated into the PEO matrix, these properties can be harnessed for applications in optoelectronics, UV shielding, and photovoltaic [5-10].

PEO-ZnO nanocomposites are expected to exhibit great potential in the field of biomedical engineering. Owing to the biocompatibility of PEO combined with the antimicrobial properties of ZnO nanoparticles, these nanocomposites are suitable for various biomedical applications, including drug delivery systems, wound healing, and tissue engineering. Moreover, PEO-ZnO nanocomposites have shown great potential in the field of biomedical engineering. Owing to the biocompatibility of PEO combined with the antimicrobial properties of ZnO nanoparticles, these nanocomposites are suitable for various biomedical applications, including drug delivery systems, wound healing, and tissue engineering.

As research in this field continues to progress, it is expected that PEO-ZnO nanocomposites will play a significant role in shaping the future of nanotechnology and its applications in diverse industries. Therefore, the objective of the present investigation was to study the structural, electrical and optical properties of ZnO nanoparticle-embedded PEO nanocomposites.

MATERIALS AND METHODS

Materials

Poly(ethylene oxide) powder (AMW: 1,00,000, freezing point 229°C) was purchased from Sigma Aldrich, India. ZnO NPs (mean diameter 10-15nm, *purity>99%)* were purchased from Ad-Nano Technologies Pvt.. High-quality polypropylene Petri-dishes (60mm) were purchased from Polylab, India, and double distilled water was purchased from Molychem laboratories.

Preparation of PEO-ZnO Nanocomposites

The solution casting method was employed to prepare the PEO-ZnO nanocomposite films. Three grams of poly (ethylene oxide) was dissolved in double distilled water (30ml) and stirred magnetically at 600 rpm for 48hours at room temperature to obtain a homogeneous solution. The homogeneous viscous solution was transferred to a polypropylene Petri dish. The solution was allowed to dry at ambient temperature. PEO films were obtained in four weeks with a thickness of approximately 0.33mm. Composite films with 5, 10 and 15 wt.% ZnO dispersed in PEO matrix were also prepared similarly.

Initially, 5wt.% ZnO NPs were dispersed in double distilled water (30ml) and stirred magnetically for 2 hours at room temperature. The ZnO solution and PEO solution were mixed and stirred magnetically for 48 hours. The solution was transferred to a polypropylene Petri dish, and the air bubbles were removed by shaking. The solution was allowed to dry at ambient temperature, as shown in Figure 1(a). After evaporating the solvent, we obtained a homogeneous film in approximately four weeks. This procedure was repeated to synthesize nanocomposite films with 10 and 15 wt.% ZnO. Table 1 shows the weight percent (wt.%) of ZnO for the composite films prepared in this study.

Characterization Techniques

The crystalline structure of PEO strongly influences its mechanical, thermal, and electrical properties. The XRD analysis of PEO was performed using a high-resolution X-ray diffractometer (Bruker D-8 Advance) equipped with a copper (Cu) K_α radiation source (λ = 1.5406 Å). The XRD measurements were conducted in the 2θ range of 5° to 80° with a step size of 0.02°. SEM imaging was performed using a field emission scanning electron microscope (Quanta250 FEG FEI) operated at an accelerating voltage of 10 kV. The FTIR spectra of the PEO films were recorded using a SHIMADZU-8400S FTIR Spectrometer. The spectra were collected in the mid-infrared region (4000-400cm-1) with a resolution of 4 cm^{-1}. The DC electrical conductivity studies were performed by using a 4-probe DC electrical conductivity system equipped with a heating chuck. A UV–Vis spectrometer (SHIMADZU UV–1800 series) in the 190-1100nm range was used to obtain the absorption data.

RESULTS AND DISCUSSIONS

XRD Analysis

The typical X-ray diffraction patterns for pure PEO & PEO-ZnO nanocomposites incorporated with 5, 10 and 15 wt.% ZnO NPs as shown in Figure 1(b). The XRD pattern of pure PEO shows a huge precise diffraction peak at a scattering angle of 19°<2θ<20°, representing a *d* spacing value of 0.45 nm, which is a distinctive result for a *high-molecular-weight* amorphous polymer [6-9]. XRD pattern of the composite films shows small sharp peaks at 2θ=25.92° and 25.74° for the other nanocomposites, which correspond to the diffraction peaks associated with the ZnO NPs. Figure 1(b) shows that the wide peak of the PEO polymer widens with increasing ZnO NP concentration. This result demonstrated the increased amorphous phase content of the composite films compared to that of pure PEO [9].

The pure PEO and PEO-ZnO nanocomposites revealed another wide and less-intensity crystalline peak at 2θ ~ 42°. After ZnO NPs embedded into PEO matrix, the XRD pattern of the resulting nanocomposites revealed only PEO diffraction peaks. This demonstrated that the ZnO NPs in the PEO were dispersed uniformly and homogenized. No changes are observed in the PEO matrix structure after the ZnO NPs are mixed [1-5,10] because of presence of enormous number of *hydroxyl* groups in its backbone. It was demonstrated by the purity and formation of nano-ZnO incorporated composites.

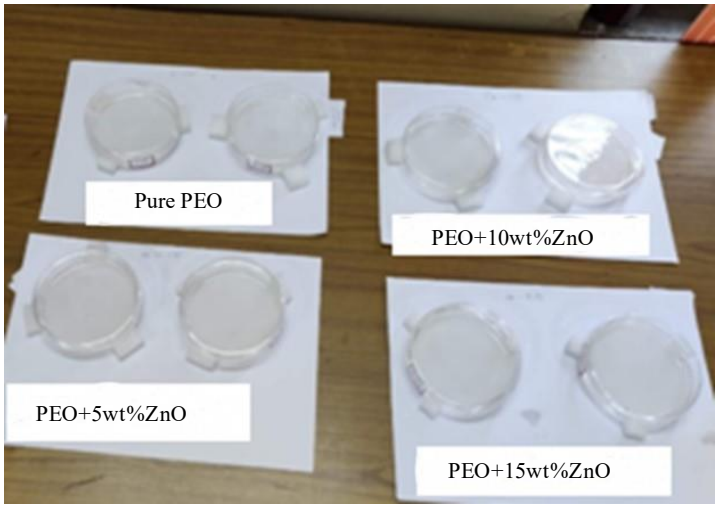

Figure 1(a). Samples after dried at ambient Temperature.

Table 1. Composition of ZNO in the PEO polymer matrix for PEO-ZNO nanocomposite films.

S.N.	Sample	Values of x (wt. (%)	Contents of PEO (g)	Contents of ZNO nanoparticles (g)
1	PPE 0	0	3	0
2	ZP 05	5	3	0.15
3	ZP 10	10	3	0.3
4	ZP 15	15	3	0.45

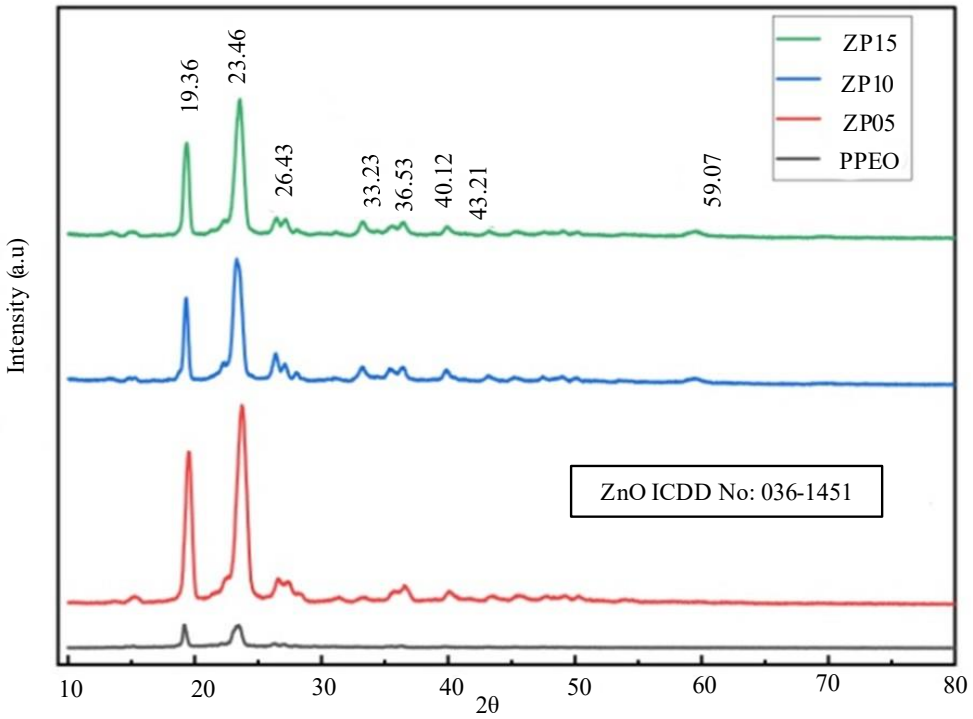

Figure 1(b). XRD patterns of PEO-ZnO nanocomposite films with varying wt.% ZnO NPs.

Surface Morphology

Scanning electron microscopy

In the case of ZnO-loaded polyethylene oxide (PEO) nanocomposite films, SEM analysis can provide information about the dispersal of nano-ZnO within the PEO matrix and the overall film morphology. SEM images of the nanocomposite films revealed the size, shape, and distribution of the ZnO nanoparticles. The occurrence of well-dispersed nanoparticles throughout PEO matrix indicated homogeneous distribution and good compatibility among the ZnO nanoparticles and the polymer matrix.

Additionally, SEM analysis can provide insights into the surface roughness and porosity of a film and the presence of any agglomerates or defects. The images obtained from SEM can help evaluate the structural integrity of the film and the impact of the nano-ZnO on surface properties of film. Furthermore, SEM analysis can be used to examine the interfacial interactions between the nano-ZnO and PEO matrix. By observing interface among the nanoparticles and polymer matrix, it is possible to assess the level of adhesion and the formation of any interfacial layers or chemical bonding.

Figure 2(b-d) shows "*SEM images*" of the PEO-ZnO nanocomposites taken at approximately the same magnification for different amounts of added ZnO during PEO. Across-view of the samples indicated that the samples were composed of spherical particles within the PEO polymer matrix. It is evident from the SEM images that nano-ZnO are agglomerated comparatively.

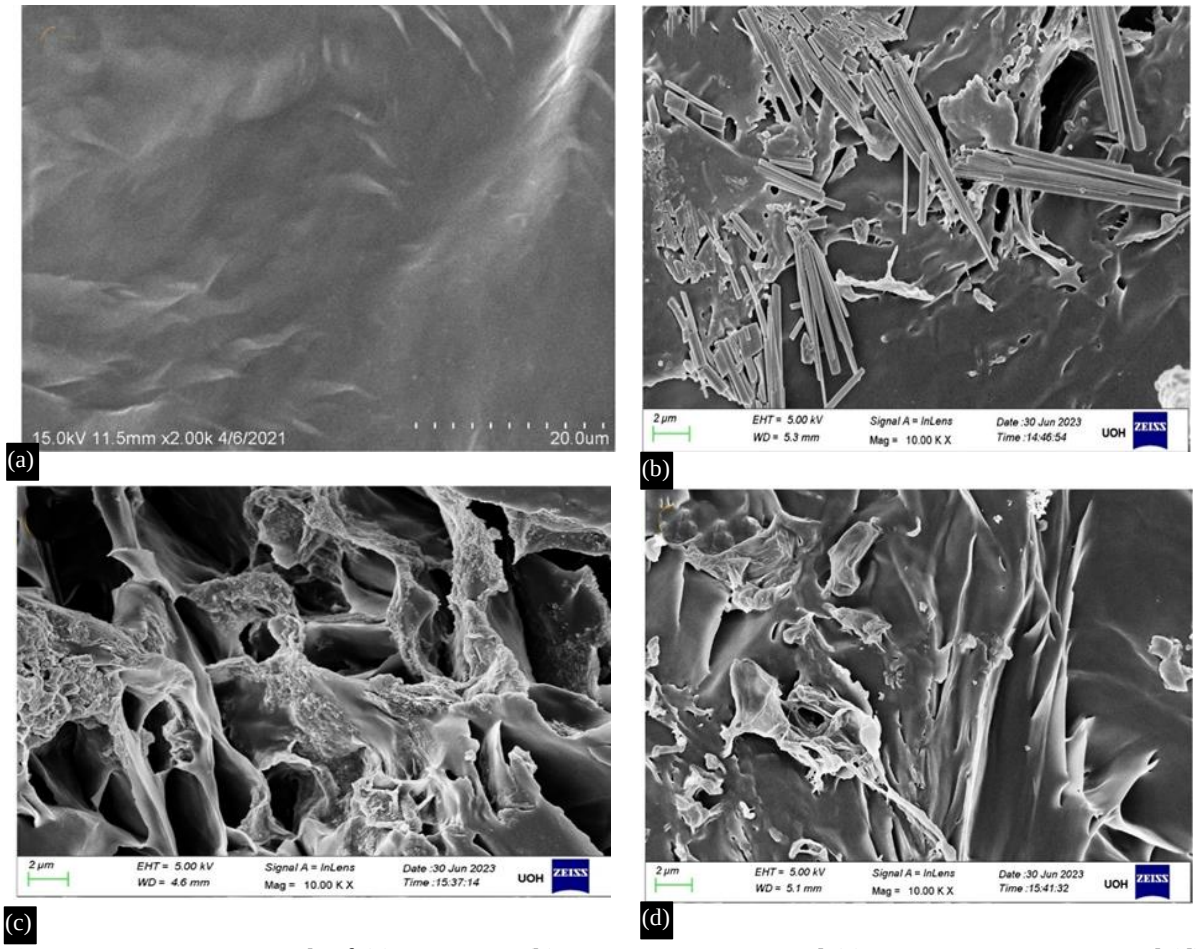

Figure 2. SEM micrograph of (a) pure PEO (b) PEO +5 wt% Zno and (c) PEO + 10 wt % Zno and (d) PEO + 15 wt % Zno at approximately the same magnification.

The EDS spectra of the PEO-ZnO nanocomposites are shown in Figure 3(a-c). It is evident from all samples that the phase of ZnO is evidently acknowledged. However, the weight percentages of carbon, zinc and oxygen found in the EDS spectrum confirm the validity of the chemical constituents. As a result, elemental analysis was used to evaluate the presence of various constituents in the ZnO NPs. The stoichiometric ratio of zinc to oxygen is approximately 1:1 in the PEO-ZnO nanocomposites.

Transmission Electron Microscopy Studies

TEM images and histogram pertaining to size distribution of particles of PEO-ZnO nanocomposites are displayed in Figure 4 (a-b). ImageJ software was employed to determine the particle sizes of nanocomposites. TEM images of the PEO-ZnO nanocomposites reveal the spherical structure of ZnO. The particle sizes of ZnO nanoparticles were evaluated using ImageJ software. The diameter of the ZnO nanoparticles is between 10 and 25 nm. These results match well with the XRD data.

Figure 4(a) is a transmission electron micrograph of PEO that has been mixed with 10 percent by weight of ZnO. There is a PEO layer enclosing the ZnO in its whole, as is shown. This is visible around the ZnO. The fact that the nanostructure of ZnO/PEO is identical to that of a core-shell nanostructure is an intriguing aspect of the TEM image. In this particular nanostructure, ZnO serves as the spherical core, while PEO serves as the spherical shell. Due to the core-shell nanostructures found in the nanostructures that are the subject of this study, there is a chance that they could become useful raw materials for the manufacture of sensors in the future. This possibility results from the characteristics that these nanostructures possess. After *oxidative polymerization* procedure concludes, PEO layer is generated on top of the ZnO nanostructure. As a result of this procedure, a spherical nanostructure is created.

Element	Weight%	Atomic%
C K	49.33	56.94
O K	49.36	42.78
Zn K	1.31	0.28
Totals	100.00	100.00

PEO+5 wt.% ZnO

(a)

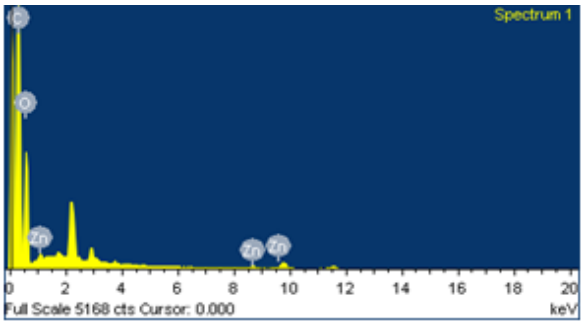

Element	Weight%	Atomic%
C K	47.15	56.71
O K	46.36	41.86
Zn K	6.49	1.43
Totals	100.00	100.00

PEO+10 wt.% ZnO

(b)

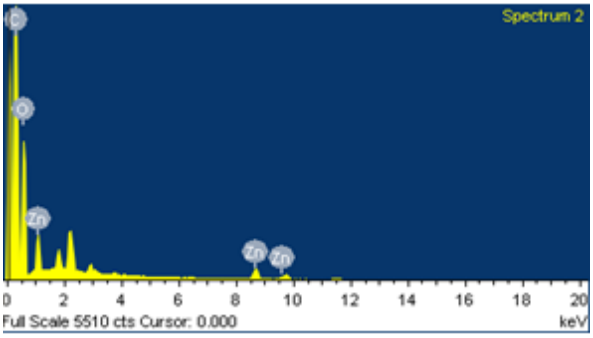

Element	Weight%	Atomic%
C K	53.37	63.74
O K	38.44	34.47
Zn K	8.18	1.80
Totals	100.00	100.00

PEO+15 wt.% ZnO

(c)

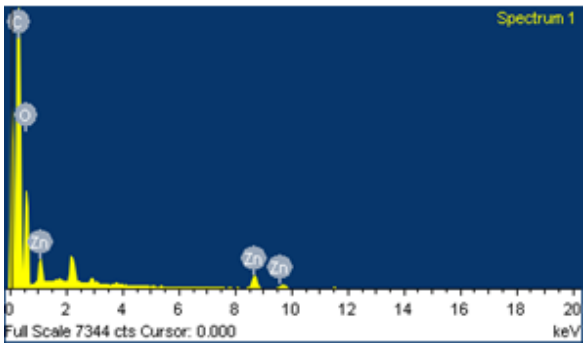

Figure 3. EDAX elemental analysis of PEO-ZnO nanocomposites.

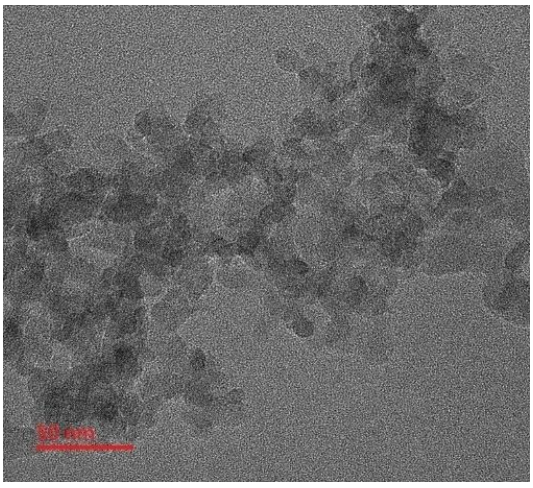

(a)

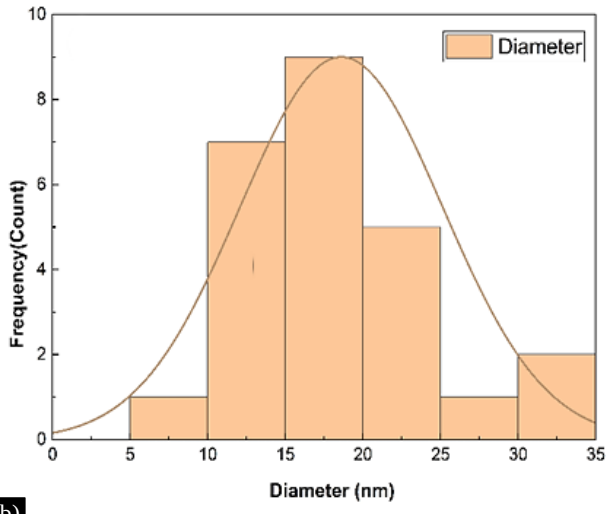

(b)

Figure 4. (a) TEM image Figure 4. (b) histogram of PEO -10 wt % Zno nanocomposites films.

Selected Area Electron Diffraction (SAED)

Since SAED analysis is simple to do and provides a wealth of data, it is frequently used to investigate a variety of materials.

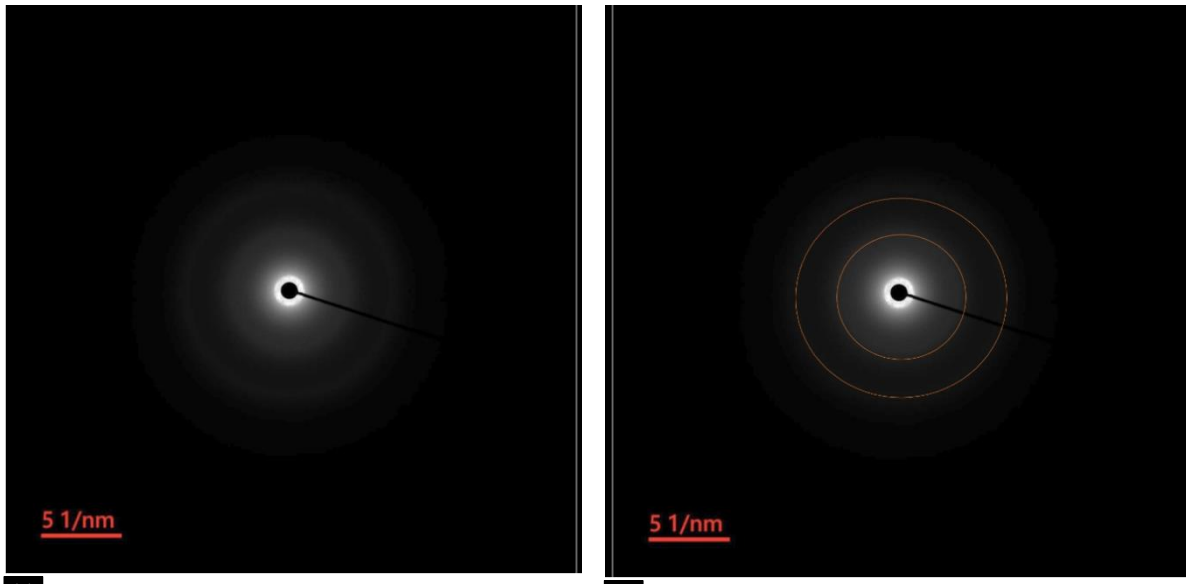

Figure 4. (C) SAED pattern of PEO -10 wt % Z no nanocomposite.

Figure 4(c) depicts the SAED patterns of the PEO based nanocomposite that contained 10 Wt% of ZnO. In addition to the darkness of the background, the patterns show that there are different circular annular rings. The SAED pattern does not have any bright spots in the image, only annular rings were observed in the pattern. Hence, the SAED patterns indisputably indicated the presence of circular annular rings, which is evidence that the composite does, in fact, have a semi crystalline or amorphous structure.

Fourier Transform Infrared (FTIR) Spectroscopy

Figure 5 shows the FTIR spectra of PEO-ZnO nanocomposite films. The *broad peak* at 3460cm^{-1} is possibly endorsed to the -OH stretching vibrations of water molecules. The *peaks* at 2922 cm^{-1} and 2857 cm^{-1} are ascribed to *anti-symmetric* and *symmetric* vibrations of –CH_2 groups of hydrocarbons present. The peak at 1627 cm^{-1} is assigned to the bending vibrations of water molecules. The peaks at 1447 cm^{-1} and 1399 cm^{-1} are due to -CH_3*bending* deformation.

The *intense peak* observed at 1109 cm^{-1} signifies the C-O stretching vibration of absorbed water. The peak at 1028 cm^{-1} is attributed to the C-N stretching vibrations of the *aliphatic amines*. The *peak* observed at 681 cm^{-1} signifies Zn–O stretch.

Table.2. The wave numbers and corresponding functional groups of the PEO-ZNO nanocomposite.

S.N.	Wave number (c m$^{-1)}$	Functional groups
1	3460	-OH, stretching of water molecule
2	2922, 2857	Anti symmetric and symmetric vibrations of the -CH_2 Groups of the hydrocarbons
3	1627	Behind vibrations of water molecule
4	1447 1399	CH_3 bending deformation
5	1109	CO stretching vibration of absorbed methanol
6	1028	CN stretching vibrations of the aliphatic amines
7	681	Zn-O stretching

UV-Vis Spectroscopy Studies

Absorption and absorption coefficients

The pure PEO film shows less absorption in the *visible range*, while nanocomposites shows *high absorption* from *visible light to UV range*, as shown in Figure 6(a). In addition, as wavelength decreases, absorbance of nanocomposite film enhances significantly. After ZnO NPs are uniformly dispersed in the PEO polymer, their UV absorption properties can be fully exploited. In addition, the composite film showed higher transparency in visible light region from 400nm to 800nm [11]. Therefore, the fabricated composite films have good UV radiation protection properties, and their transparency decreases in the visible light range with increasing ZnO nanoparticle content. The above results show that the fabricated nanocomposite films absorb a broad *range of radiation*.

The *absorption edge* of composite films shifted from 237 nm (for pure PEO) to 251nm. The *absorption edge* of composite film shifts to longer wavelengths with increasing ZnO NP concentration, which indicates the semi-crystalline phase of PEO and formation of new bonds in composite film. The *wavelength* variation indicated hydrogen bonding between the Zn^{2+} ions of ZnO and the *–OH groups* of PEO. The absorption spectrum of the composite film with 5.0 wt.% ZnO showed absorption peaks at 247-280 nm, while that of 15.0 wt.% ZnO was at 244-348 nm. These absorption bands are assigned to the n-p* and p-p* transitions, respectively. These electronic transitions indicate the existence of unsaturated *C=O or C=C bonds* mainly at the tail end of the *pure PEO polymer*.

In addition, acetyl C=O and C-O-C ring electrons are present at backbone of polymer and all these functional groups are involved in intra-molecular and intermolecular hydrogen bonding [1].

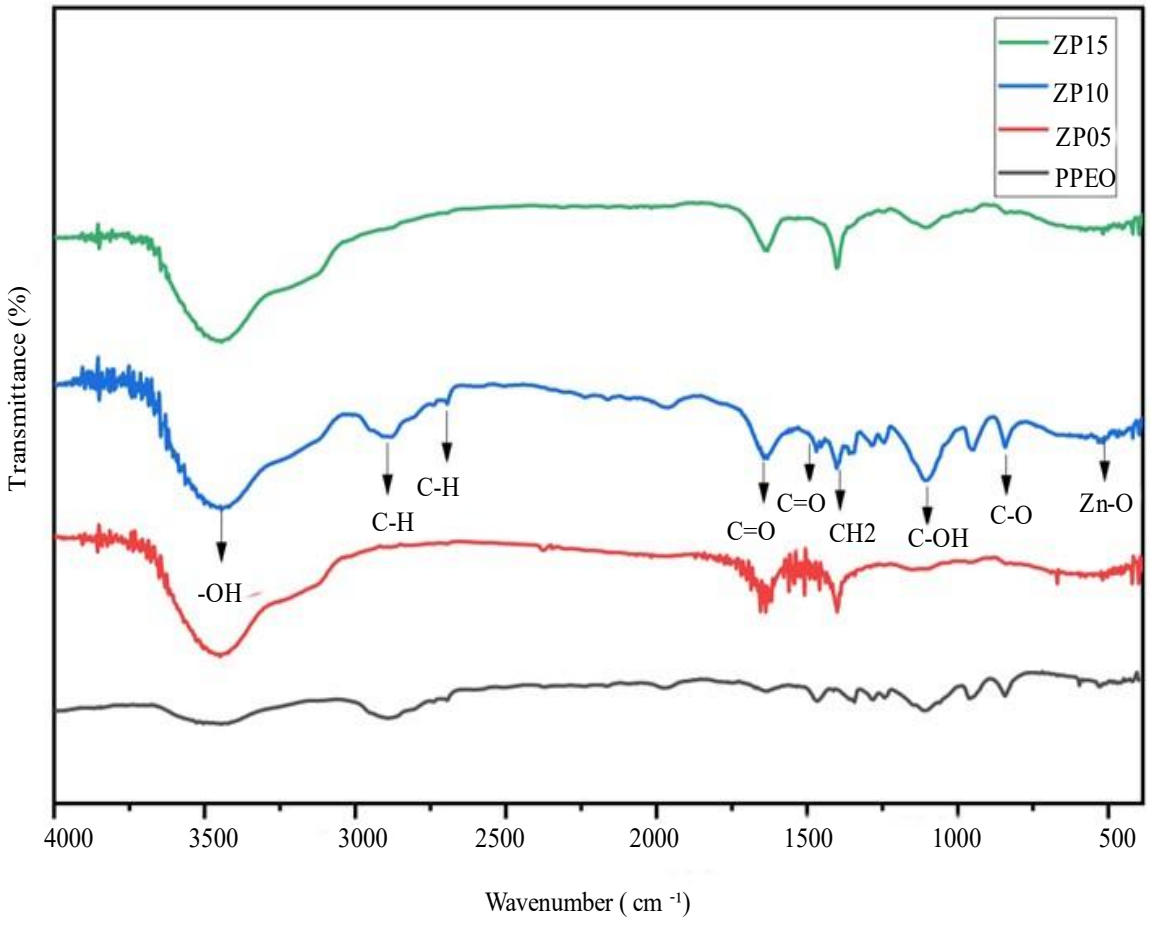

Figure 5. Representative FTIR spectra of PEO-ZnO nanocomposite films.

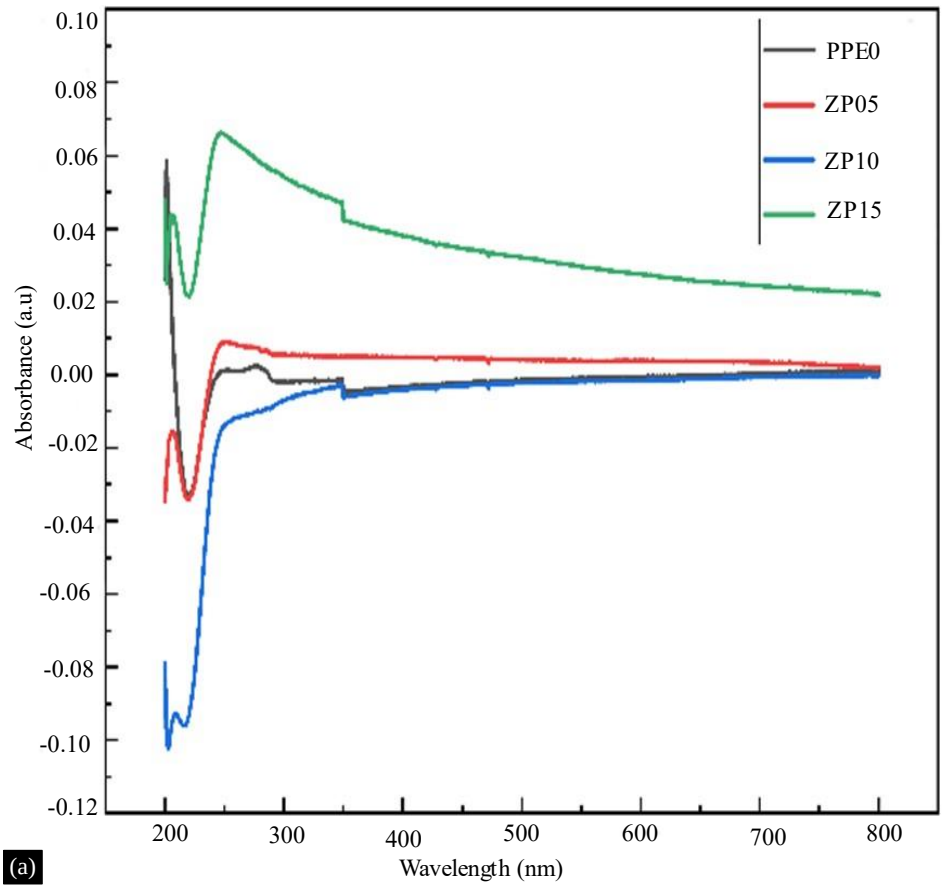

Figure 6. (a) Variation in the absorbance of PEO-ZnO nanocomposite films with respect to wavelength.

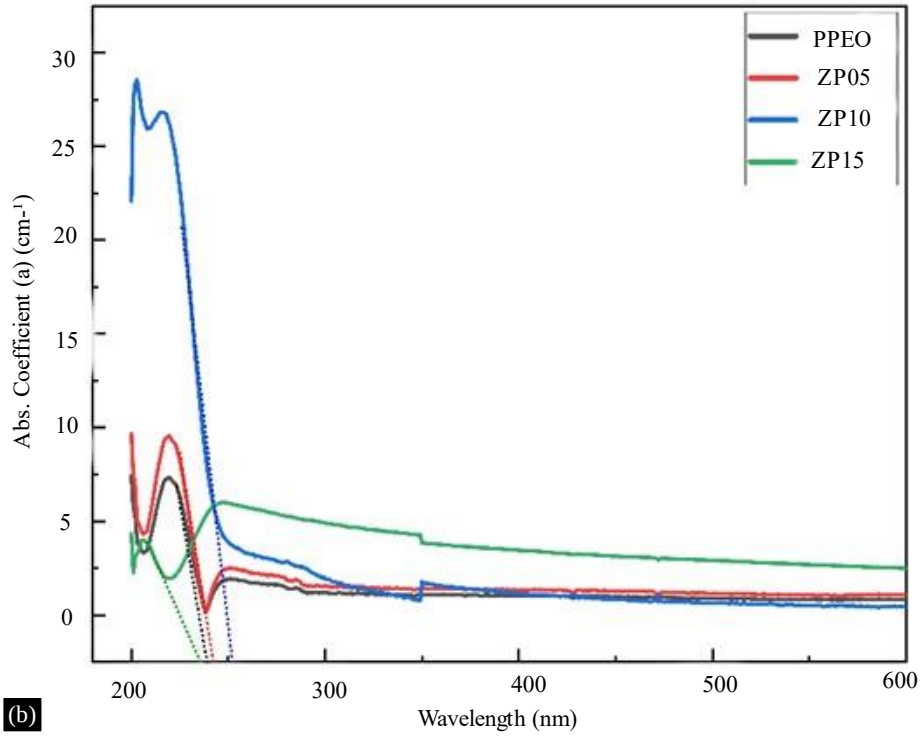

Figure 6. (b) Variation in the absorption coefficient of PEO-ZnO nanocomposite films with Wavelength.

Optical Energy Band gap

UV–Vis spectra can be used to calculate the band gap of the composite films using the *Tauc equation* [16-20].

$$[\alpha h\nu]^n = k[h\nu - E_g] \quad (1)$$

where α - absorption coefficient, $h\nu$ - incident photon energy, k - energy-independent constant, E_g - optical band gap energy, and n - exponent equal to ½ for the allowed indirect band gap transition and 2 for the allowed direct band gap transition [17]. Plot of $(\alpha h\nu)^2$ against photon energy was drawn, direct band gap transition energy was calculated from the plot, as shown in Figure 7(a). By adding just 5.0 wt.% ZnO NPs to PEO, the direct band gap was reduced from 5.21 eV (of pure PEO) to 5.18 eV. The indirect band gap energy is estimated using the $(\alpha h\nu)^{1/2}$ vs photon energy (hν) graph, as revealed in Figure 7(b). The indirect band energy was reduced to 5.08 eV from 5.03 eV (pure PEO) with the addition of 5.0 wt.% of ZnO NPs to the PEO. The *band gap energy* values of the nanocomposites are provided in Table 3.

It is also observed that by increasing the wt.% ZnO NPs in PEO, the direct band gap and indirect gap were altered to lower values. Inclusion of ZnO NPs in matrix of polymer induces additional local imperfection states in the optical band that be able to effectively alter valence and conduction band edges. This could be the core reason for the reduction in the band gap in the composites. The formation of complexes due to the interaction between the Zn^{2+} ions of ZnO and the hydroxyl groups of the polymer also modified the energy states of pure PEO [11].

Urbach Energy

The Urbach energy (E_u) was evaluated using the following equation [18]:

$$\log \alpha = \log c + \frac{h\nu}{E_u} \quad (2)$$

where C be a constant. Urbach energy (E_u), can be realized from slope of the line of plot ln(α) as a function of incident *photon energy* (hν).

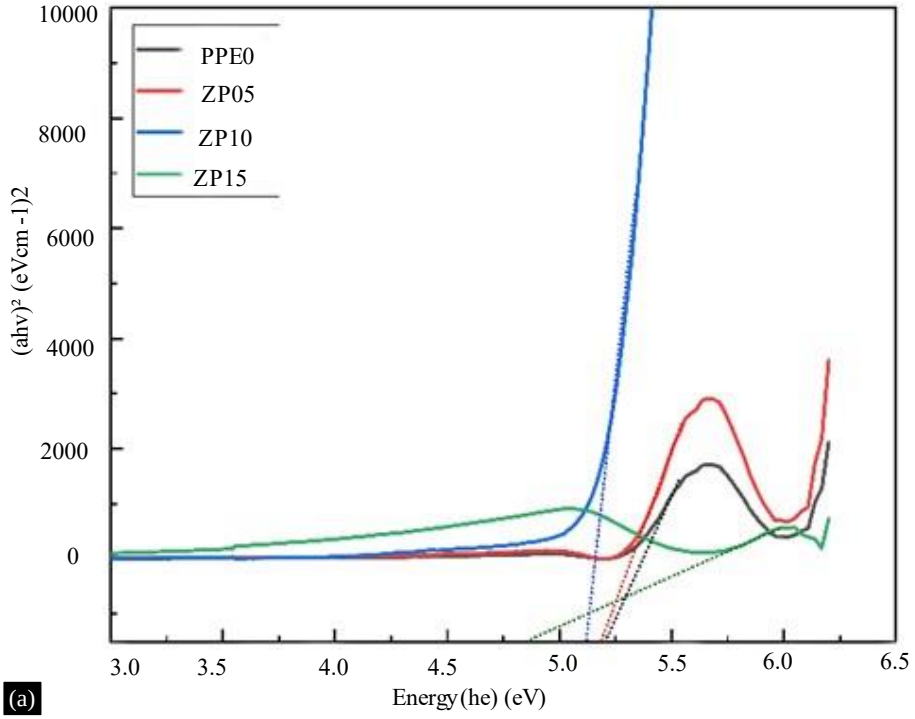

Figure 7. (a) Optical direct band gap of PEO-ZnO nanocomposite films.

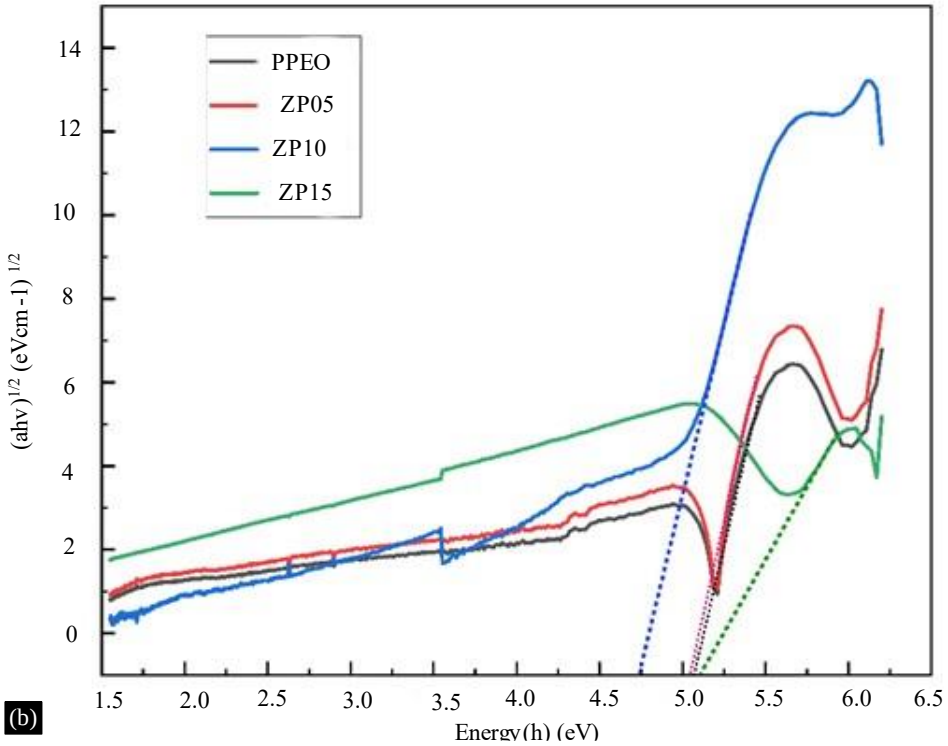

Figure 7. (b) Optical indirect band gap of PEO-ZnO nanocomposites.

When loaded with a ZnO NP content of 5 wt.%, the E_u value Slightly reduced to 1.05eV from 1.06eV (pure PEO), and the E_u values are indexed in Table 3. Urbach energy initially raised and then reduced with increasing ZnO NP concentration, indicating a low level of crystallization and disturbance of the phonon state in the polymer nanomaterials. It is also subjective by following factors: the impurity level in middle of the optical band gap, structural disorder, inhomogeneous strain and extraction absorption [13]. As seen from results, variation in Urbach energy is inverse to change in the band gap.

Table 3. Absorption edge Direct & Indirect bandgap and urban energy values of pure PEO and PEO zno nanocomposite films.

S.N.	Composite	Absorption edge (nm)	Direct band gap (ev)	Indirect band gap (ev)	Ur back energy (ev)
1	PPEO (Pure PEO)	237	5.21	5.08	1.06
2	ZP 05 (PEO+5 wt % Zno)	242	5.18	5.03	1.05
3	ZP 10 (PEO+10 wt % Zno	251	5.11	4.72	0.92
4	ZP15 (PEO+15 wt % Zno)	235	4.87	5.12	1.054

DC Conductivity Studies

The temperature dependence of ionic conductivity for different compositions of PEO nanocomposites is presented in Figure 9(a). The temperature is allowed to vary from 30°C to 80°C, which is a little above the melting temperature of the PEO polymer host. Figure 9(a) shows that the change in conductivity is small in the studied temperature range. The ionic conductivities of the different nanocomposite films linearly increase with temperature. The Plot of 'Log σ_{dc} vs. 1000/T' shows a linear increase in conductivity as a function of temperature. The general equation yields an Arrhenius-type behavior:

$$\sigma (T) = \sigma_o \exp(-E_a/kT) \quad (3)$$

Where σ_o = pre-exponential factor and E_a = activation energy. k = Boltzmann constant and T = temperature in Kelvin.

The increase in ionic conductivity with temperature may be owing to an increase in ionic mobility or carrier ion concentration. A conductivity (σ) jump is observed at ~ 65°C, corresponding to the semi-crystalline to amorphous phase transition of PEO polymer in polymer host. Due to phase change of polymer host, conductivity suddenly increases at melting temperature Tm. The increase in conductivity as a function of temperature is attributable to a process of hopping between coordinating locales, local structural relaxations, and segmental motions of polymer PEO [13,21-23]. The curve fitting of the linear portion below this temperature follows the Arrhenius equation (4). For PEO-ZnONCs, the Arrhenius equation is

$$\sigma(T) = 4.94 \times 10\text{-}4 \exp(-0.814/kT) \quad (4)$$

The above equation shows that the exponent in the argument of the exponential is the activation energy Ea = 0.814 eV. The relationship between the activation energy Ea and the concentration of ZnONPs is presented in Figure 10. Figure 10 shows that the activation energy is minimal for x = 5 wt.% ZnO. The low activation energy (Ea) of the PEO-ZnO NC composition confirmed the high ionic conductivity of the composite.

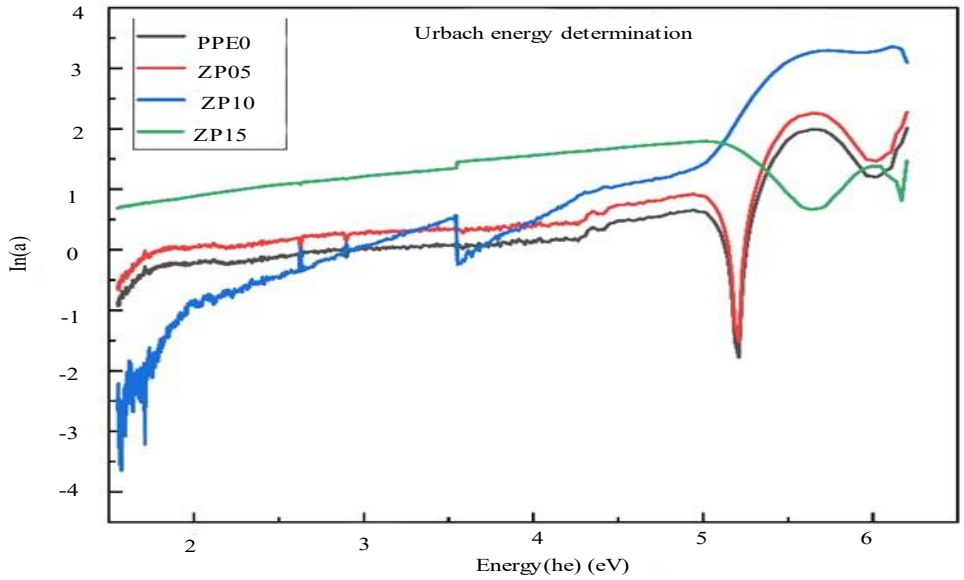

Figure 8. Urbach energy of PEO-ZnO nanocomposite films.

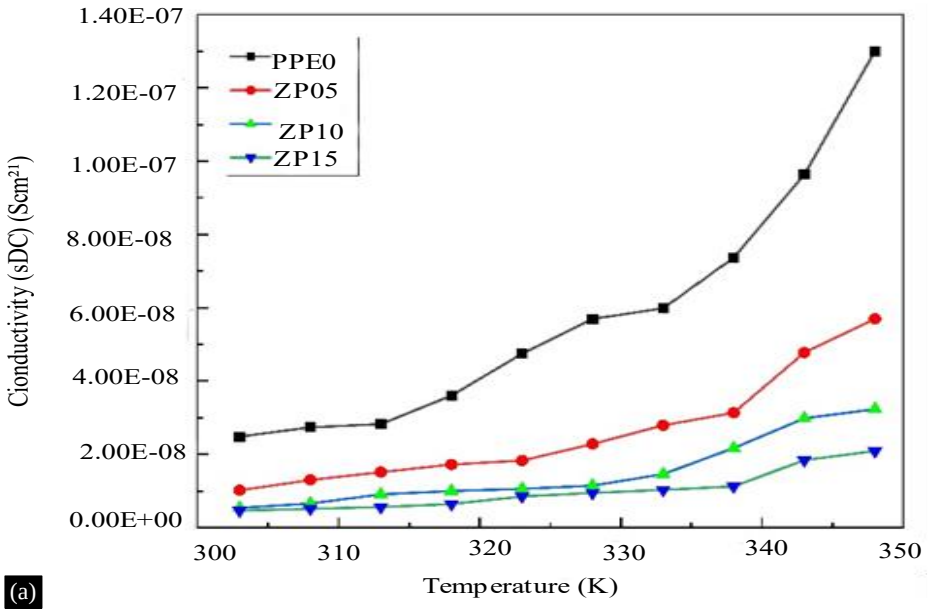

(a)

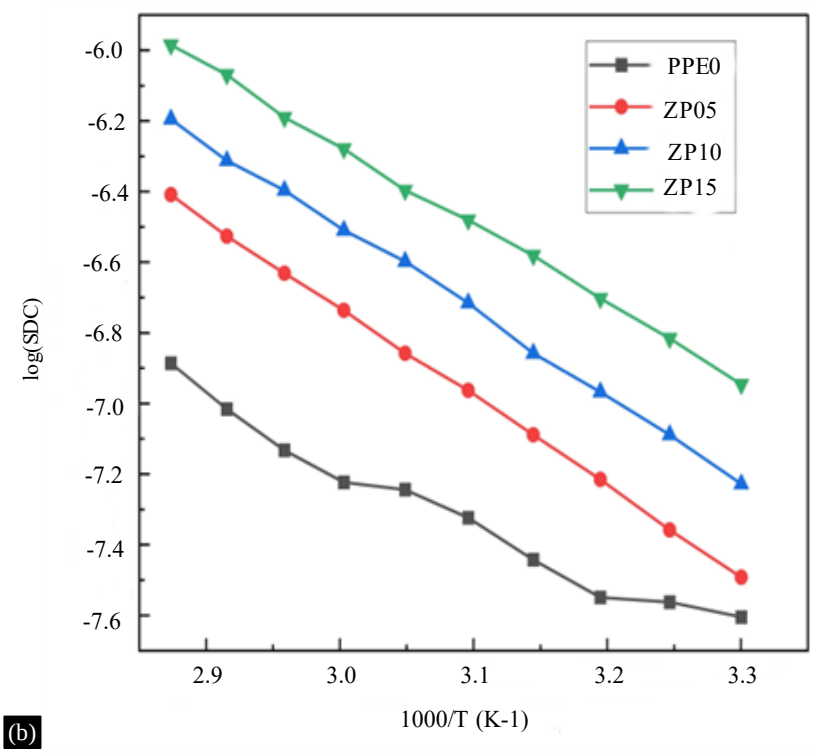

Figure 9. (a) σ_{dc}vs T and (b) log σ_{dc}vs. 1000/T plot for PEO-ZnO nanocomposites with different wt.% compositions.

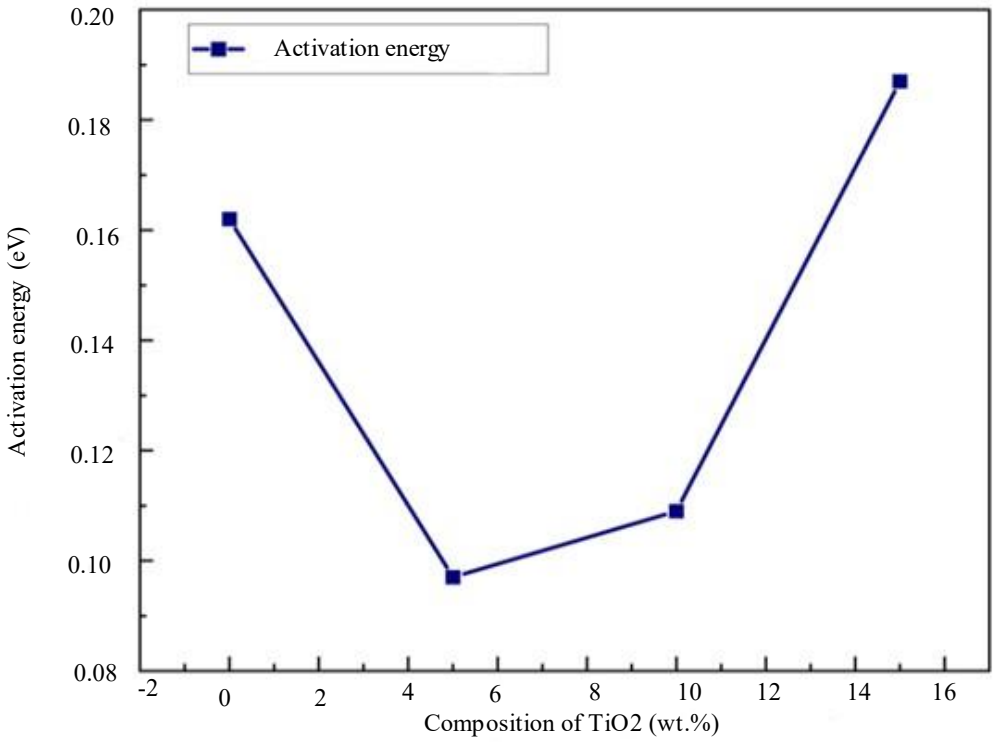

Figure 10. Activation energy E_a vs Composition of ZnO for PEO-ZnO nanocomposites.

CONCLUSIONS

The cost-effective solution casting technique was utilized to prepare PEO-ZnO nanocomposite films, which were found to be semi-crystalline in nature through XRD studies. Surface morphology studies

indicated that the film surface was smooth at lower concentrations of ZnO, and the surface roughness of the films increased with increasing weight percentage of ZnO. The FTIR studies showed that there was good interaction between the PEO polymer matrix and the ZnO nanoparticles. The direct and indirect band gaps of the composite films moved toward lower energies. The Urbach energy also confirmed the formation of defect states in the band gap region and the decreased crystalline phase with increasing ZnO concentration. The DC electrical conductivity and activation energy increased with increasing wt.% ZnO and sample temperature.

REFERENCES

1. Manjunath, A., Irfan, M., Anushree, K.P., Vinutha, K.M. and Yamunarani, N. (2016) Synthesis and Characterization of CuO Nanoparticles and CuO Doped PVA Nanocomposites. Advances in Materials Physics and Chemistry, 6, 263-273. http://dx.doi.org/10.4236/ampc.2016.610026
2. A. Paul, B. Schwind, C. Weinberger, M. Tiemann, T. Wagner, Gas Responsive Nanoswitch: Copper Oxide Composite for Highly Selective H_2S Detection. *Adv. Funct. Mater.* 2019, 29, 1904505. https://doi.org/10.1002/adfm.201904505
3. Chao Wang, Yiqian Wang, Xuehua Liu, Feiyu Diao, Lu Yuanc and Guangwen Zhouc (2014), Novel hybrid nanocomposites of polyhedral Cu_2O nanoparticles–CuO nanowires with enhanced photoactivity. Cite this: Phys. Chem. Chem. Phys., 16, 17487. DOI: 10.1039/c4cp01696c
4. Y. Li, J. Rodrigues and H. Tomas, "Injectable and Biodegradable Hydrogels: Gelation, Biodegradation and Biomedical Applications," Chemical Society Reviews, Vol. 41, No. 6, 2012, pp. 2193-2221. doi:10.1039/c1cs15203c
5. Hajipour, P.; Bahrami, A.; Mehr, M.Y.; van Driel, W.D.; Zhang, K. Facile Synthesis of Ag Nanowire/TiO2 and Ag Nanowire/TiO2/GO Nanocomposites for Photocatalytic Degradation of Rhodamine B. Materials 2021, 14, 763. https:// doi.org/10.3390/ma14040763
6. Yi Yan, Huajun Guo, Zhixing Wang, Xinhai Li, Guochun Yan, Jiexi Wang. Electrospinning-Enabled Si/C Nanofibers with Dual Modification as Anode Materials for High-Performance Lithium-Ion Batteries[J]. Acta Metallurgica Sinica (English Letters), 2021, 34(3): 329-336.https://doi.org/10.1007/s40195-020-01087-z.
7. Karakoti AS, Das S, Thevuthasan S, Seal S. PEGylated inorganic nanoparticles. Angew Chem Int Ed Engl. 2011 Feb 25;50(9):1980-94. doi: 10.1002/anie.201002969. Epub 2011 Jan 27. PMID: 21275011.
8. Magnone, E.; Hwang, J.Y.; Shin, M.C.; Zhuang, X.; Lee, J.I.; Park, J.H. Al_2O_3-Based Hollow Fiber Membranes Functionalized by Nitrogen-Doped Titanium Dioxide for Photocatalytic Degradation of Ammonia Gas. Membranes 2022, 12, 693. https://doi.org/10.3390/ membranes12070693
9. Tayel, Amr & Ramadan, Adham & Seoud, Omar. (2018). Titanium Dioxide/Graphene and Titanium Dioxide/Graphene Oxide Nanocomposites: Synthesis, Characterization and Photocatalytic Applications for Water Decontamination. Catalysts. 8. 491. 10.3390/catal8110491.
10. Dey A, Karan S, De SK (2010) Molecular interaction and ionic conductivity of polyethylene oxide-liclo4 nanocomposites. J Phys Chem Solids 71:329–335. https://doi.org/10.1016/j.jpcs.2009.12.085
11. Jiang Y, Wang WN, Biswas P, Fortner JD. Facile aerosol synthesis and characterization of ternary crumpled graphene-TiO_2-magnetite nanocomposites for advanced water treatment. ACS Appl Mater Interfaces. 2014 Jul 23;6(14):11766-74. doi: 10.1021/am5025275. Epub 2014 Jul 14. PMID: 24983817.
12. Purabgola, Anushka & Mayilswamy, Neelaambhigai & Kandasubramanian, Balasubramanian. (2022). Graphene-based TiO2 composites for photocatalysis & environmental remediation: synthesis and progress. Environmental Science and Pollution Research. 29. 10.1007/s11356-022-18983-9. DOI:10.1007/s11356-022-18983-9
13. Sreekanth T, Jaipal Reddy M, Subba Rao UV. Polymer electrolyte system based on (PEO+KBrO3) - its application as an electrochemical cell. Journal of Power Sources 2001;93:268-272. https://doi.org/10.1016/s0378-7753(00)00558-9.
14. Tan, Lling-Lling & Ong, Wee-Jun & Chai, Siang-Piao & Goh, Boon Tong & Mohamed, Abdul. (2015). Visible-light-active oxygen-rich TiO2 decorated 2D graphene oxide with enhanced photocatalytic activity toward carbon dioxide reduction. Applied Catalysis B: Environmental. 179. DOI: 10.1016/j.apcatb.2015.05.024.

15. Saravanan R, Karthikeyan S, Gupta VK, Sekaran G, Narayanan V, Stephen A. Enhanced photocatalytic activity of ZnO/CuO nanocomposite for the degradation of textile dye on visible light illumination. Mater Sci Eng C Mater Biol Appl. 2013 Jan 1;33(1):91-8. doi: 10.1016/j.msec.2012.08.011. Epub 2012 Aug 18. PMID: 25428048.
16. Shahruddin, Munawar & Zakaria, Nuratikah & Junaidi, Nurul & Alias, Nur Hashimah & Othman, Nur. (2017). Study of the Effectiveness of Titanium Dioxide (TiO2) nanoparticle in Polyethersulfone (PES) Composite Membrane for Removal of Oil in Oily Wastewater. Journal of Applied Membrane Science & Technology. 19. DOI: 10.11113/amst.v19i1.21.
17. Benchaabane, Aida & Hamed, Z. & Lahmar, Abdelilah & Sanhoury, Med Abderrahmane & Kouki, Faycal & Zellama, K. & Zeinert, A. & Bouchriha, H.. (2016). Optical properties of P3HT:tributylphosphine oxide-capped CdSe nanocomposites. Applied Physics A. 122. DOI:10.1007/s00339-016-0244-z.
18. Alzagameem A, Klein SE, Bergs M, Do XT, Korte I, Dohlen S, Hüwe C, Kreyenschmidt J, Kamm B, Larkins M, Schulze M. Antimicrobial Activity of Lignin and Lignin-Derived Cellulose and Chitosan Composites Against Selected Pathogenic and Spoilage Microorganisms. Polymers (Basel). 2019 Apr 11;11(4):670. doi: 10.3390/polym11040670. PMID: 30979077; PMCID: PMC6523900.
19. Olabisi, O., & Adewale, K. (Eds.). (2016). Handbook of Thermoplastics (2nd ed.). CRC Press. https://doi.org/10.1201/b19190
20. Lau, G.E.; Che Abdullah, C.A.; Wan Ahmad, W.A.N.; Assaw, S.; Zheng, A.L.T. Eco-Friendly Photocatalysts for Degradation of Dyes. *Catalysts* 2020, *10*, 1129. https://doi.org/10.3390/catal10101129
21. Patil, M. & Lakshminarasimhan, S.N. & Santhosh, Gopika. (2021). Optical and thermal studies of host Poly (methyl methacrylate) (PMMA) based nanocomposites: A review. Materials Today: Proceedings. 46. DOI:10.1016/j.matpr.2021.01.840.
22. Benchaabane, Aida & Hamed, Z. & Lahmar, Abdelilah & Sanhoury, Med Abderrahmane & Kouki, Faycal & Zellama, K. & Zeinert, A. & Bouchriha, H.. (2016). Optical properties of P3HT:tributylphosphine oxide-capped CdSe nanocomposites. Applied Physics A. 122. DOI:10.1007/s00339-016-0244-z.
23. Yang, Wei & Song, Shuangshuang & Zhang, Chaoqun & Liang, Wenyao & Dong, Xianming & Luo, Ying & Cai, Xin. (2017). Enhanced photocatalytic oxidation and biodegradation of polyethylene films with PMMA grafted TiO2 as pro-oxidant additives for plastic mulch application. Polymer Composites. 39. DOI:10.1002/pc.24358.

